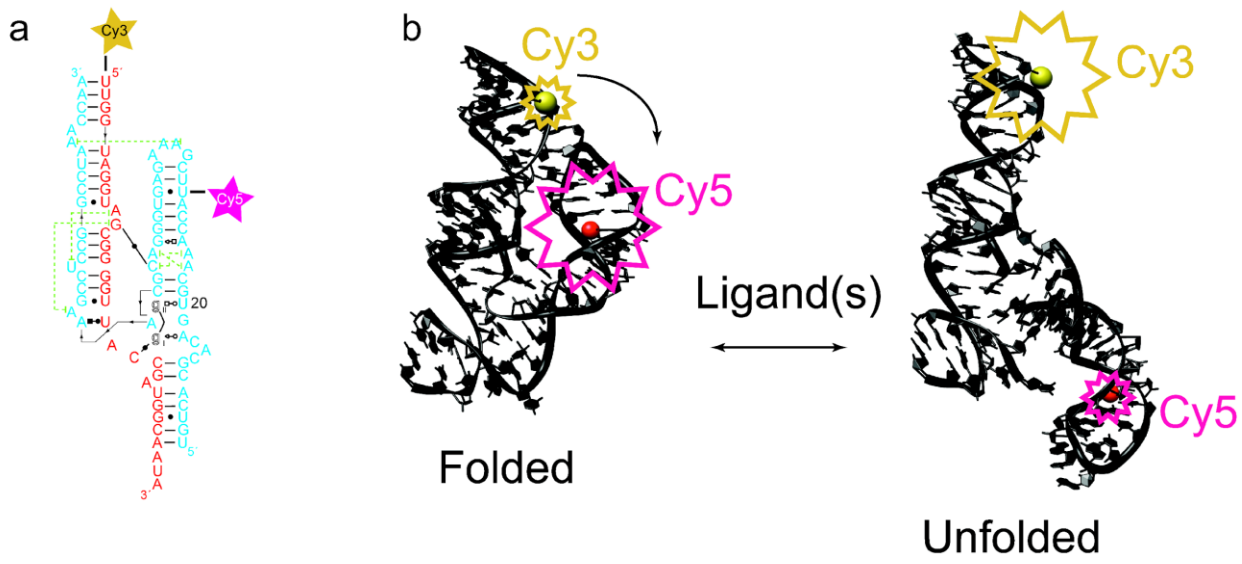


**Supplementary Figure 1.** Structural models and fluorophore locations. (**a**) Secondary structure diagram depicting the two-strand construct of the c-di-GMP riboswitch used in this study[1]. Green dotted lines represent stacking interactions. The cognate ligand is represented by black outlined lowercase letters. The red strand contains a Cy3 dye on its 5′ end. The blue strand contains a modified base to which Cy5 is covalently attached. This riboswitch construct incorporates a G20U mutation[2], which results in approximately micromolar c-di-GMP binding affinity (**Supplementary Table 3**). (**b**) Structural models of the riboswitch in the folded and unfolded conformations, derived from X-ray crystallography (folded) and small-angle X-ray scattering data (unfolded)[3]. In the folded conformation, the dyes are brought into close proximity, giving rise to high Förster energy transfer efficiency ($E_{FRET}$). The unfolded conformation exhibits low $E_{FRET}$ due to the longer distance between the dyes.

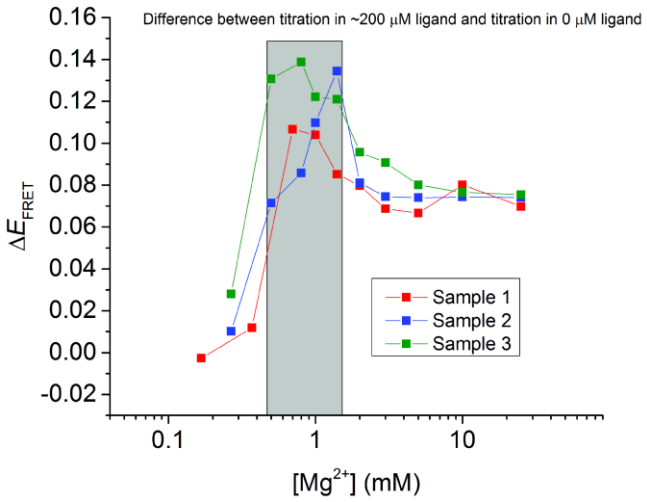


**Supplementary Figure 2.** Plot of $\Delta E_{FRET}$ across $Mg^{2+}$ concentrations. The $\Delta E_{FRET}$ was calculated by subtracting the $E_{FRET}$ signal in the absence of ligand from the $E_{FRET}$ signal in the presence of ~200 μM c-di-GMP at each $Mg^{2+}$ concentration tested. Data were obtained from different samples prepared on different days and were normalized based on their the unfolded and folded signals (**Methods**). The grey box highlights the maximal $\Delta E_{FRET}$ between the titrations (+/- ligand), which occurs around 1 mM $Mg^{2+}$.

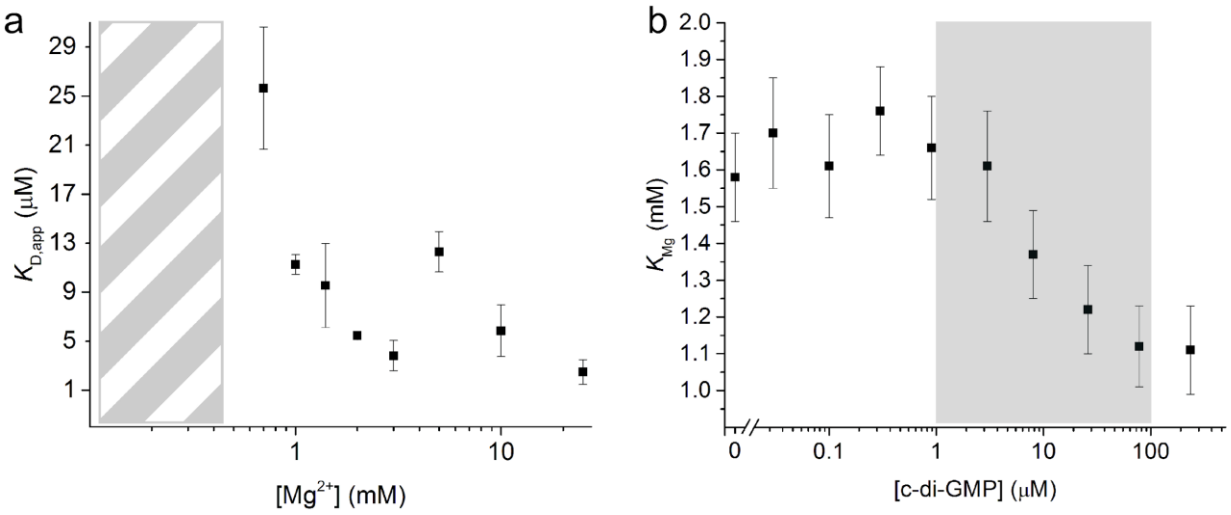


**Supplementary Figure 3.** Midpoints of $Mg^{2+}$ and c-di-GMP titrations characterize the $K_{Mg}$ and $K_{D,app}$ as a function of the orthogonal variable. (**a**) A plot of the c-di-GMP binding affinity, or $K_{D,app}$, as a function of $Mg^{2+}$ concentration. The $K_{D,app}$ is obtained from a fit to the titration using a two-state binding model (**Methods**). The error reported is the standard error of the fit. Data at the lowest $Mg^{2+}$ concentrations were not fit due to a low signal-to-noise ratio of the $E_{FRET}$ data (patterned box). (**b**) A plot of the $Mg^{2+}$ midpoint, or $K_{Mg}$, as a function of c-di-GMP concentration. The $K_{Mg}$ is obtained using a semi-empirical Hill-type fit of each $Mg^{2+}$ titration series (**Methods**). The grey box represents the 50 – 100 fold range over which the riboswitch is most responsive to changes in c-di-GMP concentration. Reported error bars are obtained from fits to the data in **Fig. 2b, c**.

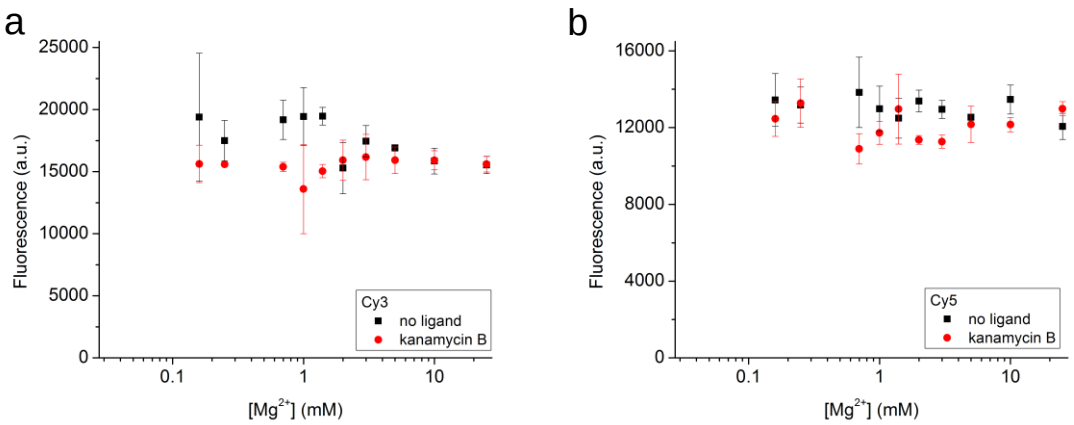


**Supplementary Figure 4**. RNA constructs labeled with a single fluorophore (Cy3, left panel; Cy5, right panel) reveal similar fluorescence intensities across a wide range of $[Mg^{2+}]$ in the absence and presence of 200 μM kanamycin B. This demonstrates that the fluorescence properties of the dyes under these conditions are not altered by the RNA conformation or the presence of kanamycin B. Each experiment was performed in triplicate and is reported as the mean ± standard deviation.

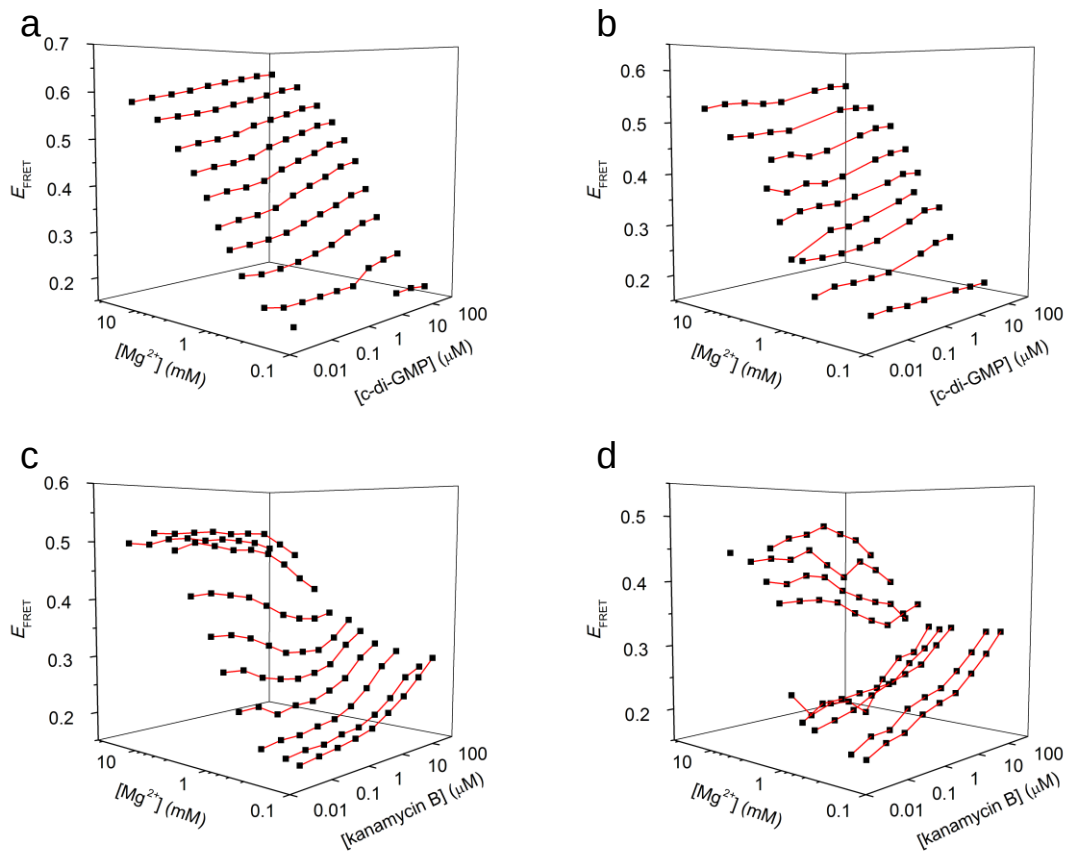


**Supplementary Figure 5**. Conformational landscapes are reproducible over multiple experiments. Key features of the landscape are observed in landscapes generated from samples prepared on different days, including the kanamycin B-induced increase in $E_{FRET}$ in low $Mg^{2+}$ concentrations and decrease in $E_{FRET}$ in high $Mg^{2+}$ concentrations. The $Mg^{2+}$ and kanamycin B conditions were varied in each experiment, precluding direct merging of the data. (**a**) Conformational landscape in the presence of cyclic di-GMP, as depicted in **Fig. 2**. (**b**) Conformational landscape in the presence of cyclic di-GMP generated from separate samples prepared on a different day than in (**a**). (**c**) Conformational landscape in the presence of kanamycin B, as depicted in **Fig. 3**. (**d**) Conformational landscape in the presence of kanamycin B generated from separate samples prepared on a different day than in (**c**).

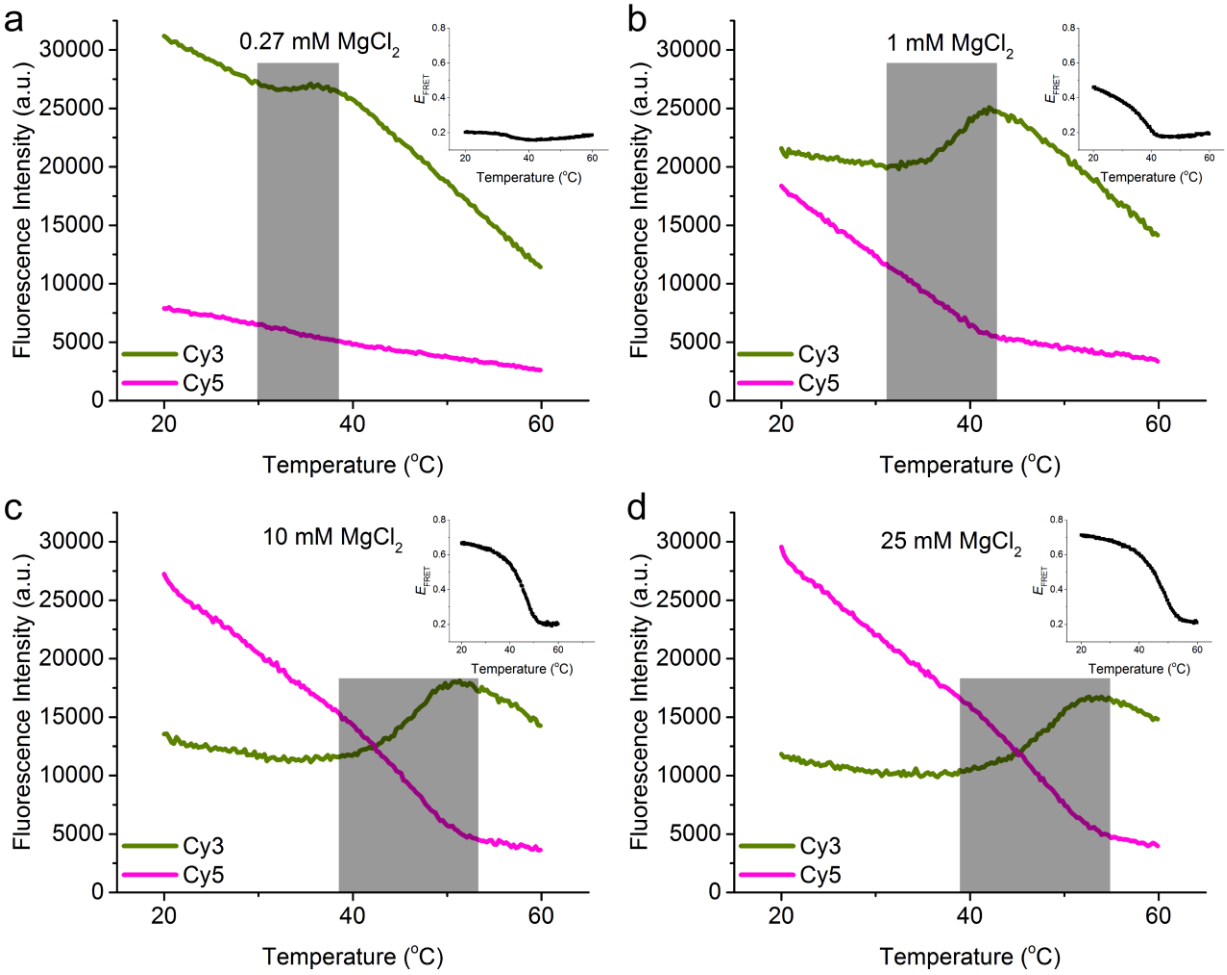


**Supplementary Figure 6.** Anti-correlated Cy3 and Cy5 signal changes during cooperative temperature-induced tertiary unfolding. Signal changes are plotted from samples in (**a**) 0.27 mM $Mg^{2+}$, (**b**) 1 mM $Mg^{2+}$, (**c**) 10 mM $Mg^{2+}$, and (**d**) 25 mM $Mg^{2+}$. Insets show the $E_{FRET}$ calculated from the Cy3 and Cy5 signal intensities across temperature (**Methods**). Unfolded RNA places the dyes far apart and very little energy transfer occurs, resulting in high donor emission (Cy3) and low acceptor emission (Cy5). Folded RNA brings the dyes in close proximity and results in low donor emission (Cy3) and high acceptor emission (Cy5) due to energy transfer. The grey shaded area in each plot represent the cooperative tertiary unfolding transition. The unfolding transition spans larger temperature ranges as the RNA is stabilized in higher $Mg^{2+}$. Following cooperative tertiary unfolding, the changes in Cy3 and Cy5 signals are dominated by photobleaching and the temperature-dependence of the quantum yield.

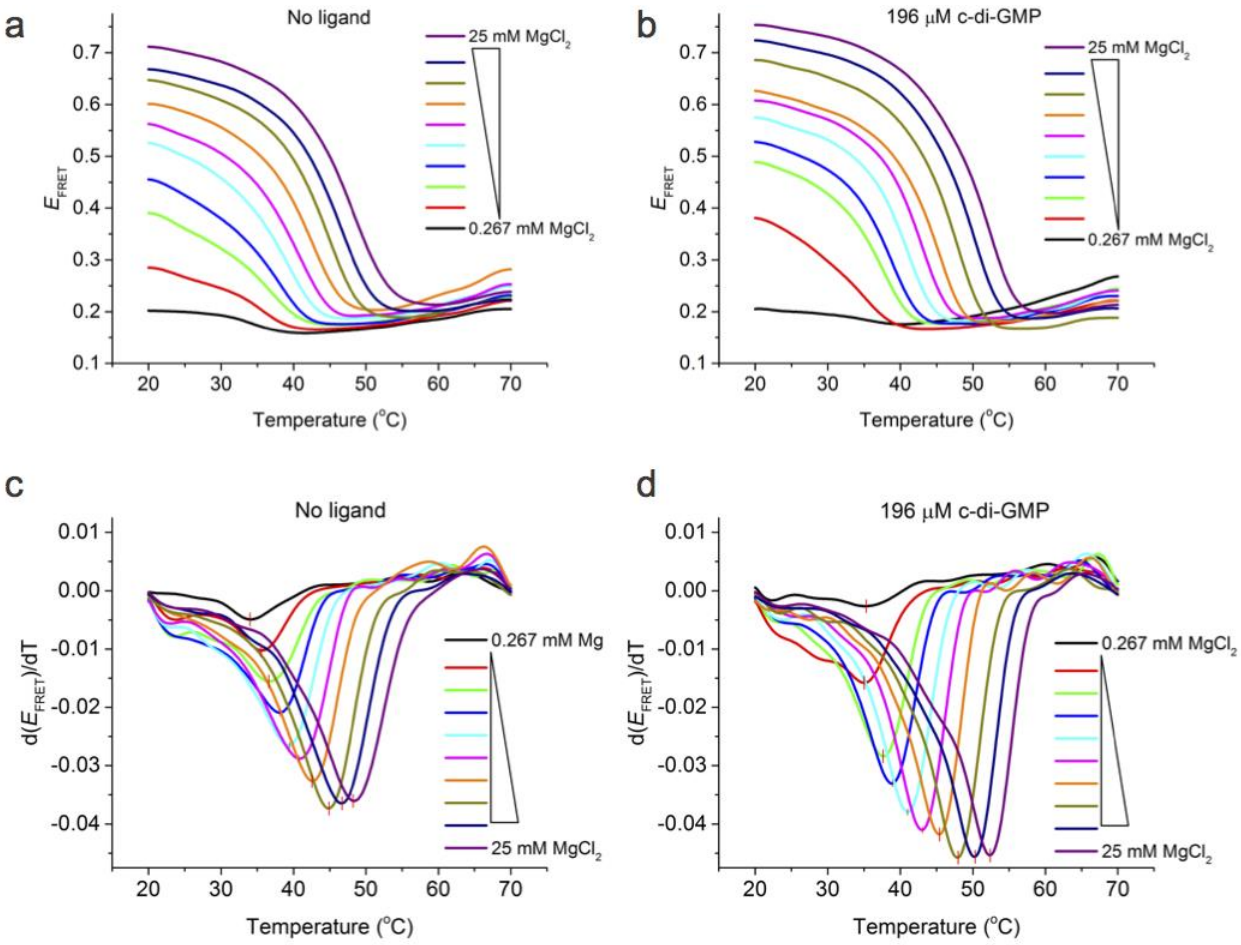


**Supplementary Figure 7.** Temperature-induced tertiary unfolding as a function of $Mg^{2+}$ and c-di-GMP. Samples were prepared in 10 different $Mg^{2+}$ concentrations (all in mM; 0.267, black; 0.5, red; 0.8, green; 1, blue; 1.4, cyan; 2, magenta; 3, orange; 5, olive; 10, navy; 25, purple). Representative $E_{FRET}$ data (**a**) in the absence of ligand and (**b**) in the presence of 196 μM c-di-GMP were smoothed with an FFT filter using a 10-point window and cutoff frequency of 0.193 (Origin 9.1). Derivative plots of the data (**c**) in the absence of ligand and (**d**) in the presence of 196 μM c-di-GMP. The $T_m^{3°}$ is determined from the negative peak of the derivative plots and is marked by a vertical red dash. The $T_m^{3°}$ increases with increasing $Mg^{2+}$ concentration and in the presence of c-di-GMP. The derivative amplitudes are larger in the presence of c-di-GMP than in the absence of c-di-GMP due to the increased raw $E_{FRET}$ signal of the c-di-GMP-bound conformation.

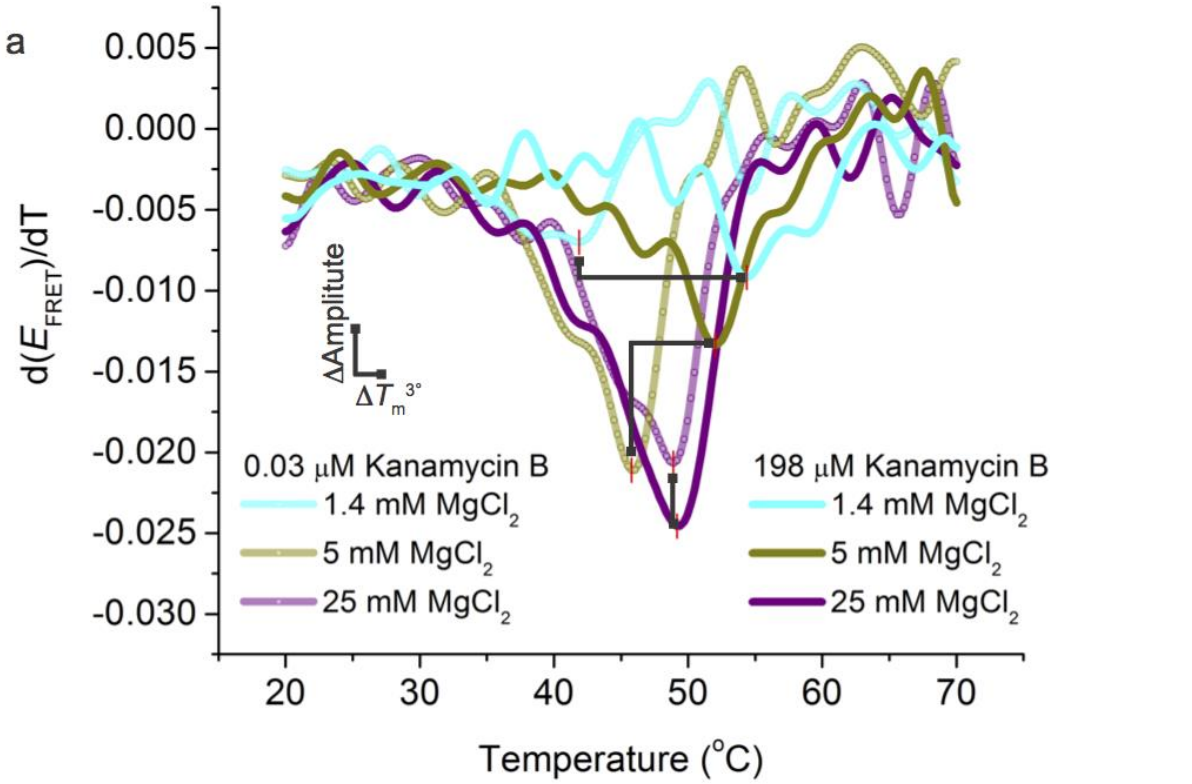
a
d(E_FRET)/dT
Temperature (°C)
ΔAmplitute
ΔT_m 3°
0.03 μM Kanamycin B
1.4 mM MgCl2
5 mM MgCl2
25 mM MgCl2
198 μM Kanamycin B
1.4 mM MgCl2
5 mM MgCl2
25 mM MgCl2

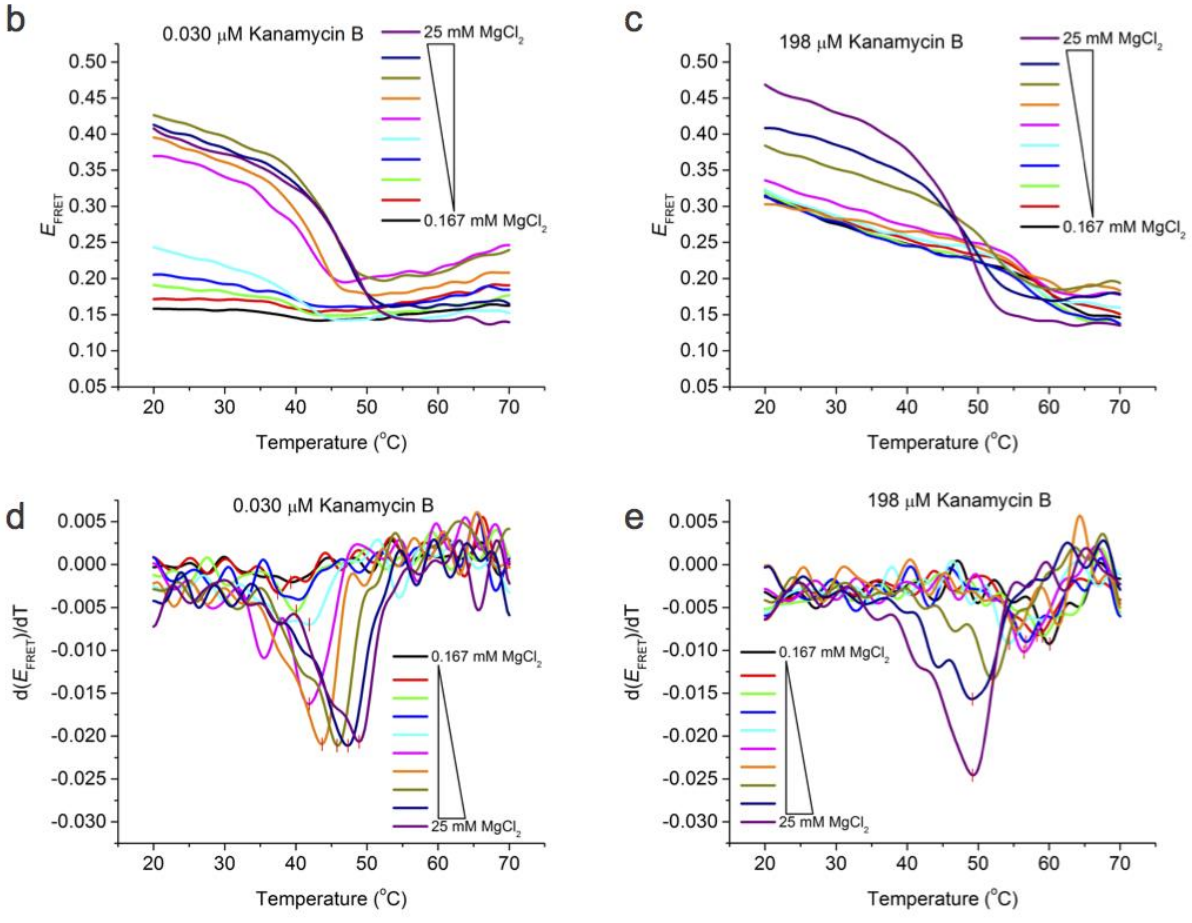
b
0.030 μM Kanamycin B
25 mM MgCl2
0.167 mM MgCl2
E_FRET
Temperature (°C)
c
198 μM Kanamycin B
25 mM MgCl2
0.167 mM MgCl2
E_FRET
Temperature (°C)
d
0.030 μM Kanamycin B
0.167 mM MgCl2
25 mM MgCl2
d(E_FRET)/dT
Temperature (°C)
e
198 μM Kanamycin B
0.167 mM MgCl2
25 mM MgCl2
d(E_FRET)/dT
Temperature (°C)

**Supplementary Figure 8.** Temperature-induced tertiary unfolding modulated by the non-cognate ligand kanamycin B. Samples were prepared in 10 different $Mg^{2+}$ concentrations (all in mM; 0.167, black; 0.25, red; 0.7, green; 1, blue; 1.4, cyan; 2, magenta; 3, orange; 5, olive; 10, navy; 25, purple). (a) Comparison of $E_{FRET}$ derivative plots at low (0.03 μM, dotted line) and high (198 μM, solid line) kanamycin B concentrations in three different $Mg^{2+}$ concentrations. The changes in amplitude and $T_m^{3°}$ are marked by the black lines and squares. At low $Mg^{2+}$ concentrations (e.g. 1.4 mM, blue) the addition of 198 μM kanamycin B increases the $T_m^{3°}$ by more than 10 ºC. The $\Delta T_m^{3°}$ is ~5 ºC in 5 mM $Mg^{2+}$ (olive) and nearly unchanged in 25 mM $Mg^{2+}$ (purple). The $E_{FRET}$ data (**b**) in 0.03 μM and (**c**) 198 μM kanamycin B were smoothed with an FFT filter using a 10-point window and cutoff frequency of 0.193 (Origin 9.1). Derivative plots of the data (**d**) in 0.03 μM and (**e**) 198 μM kanamycin B with $T_m^{3°}$ marked by a vertical red dash at the negative maximum. Comparison of panels (**d**) and (**e**) reveal that the $T_m^{3°}$ changes induced by kanamycin B are largest at low $Mg^{2+}$ concentrations but are nearly unchanged at high $Mg^{2+}$ concentrations.

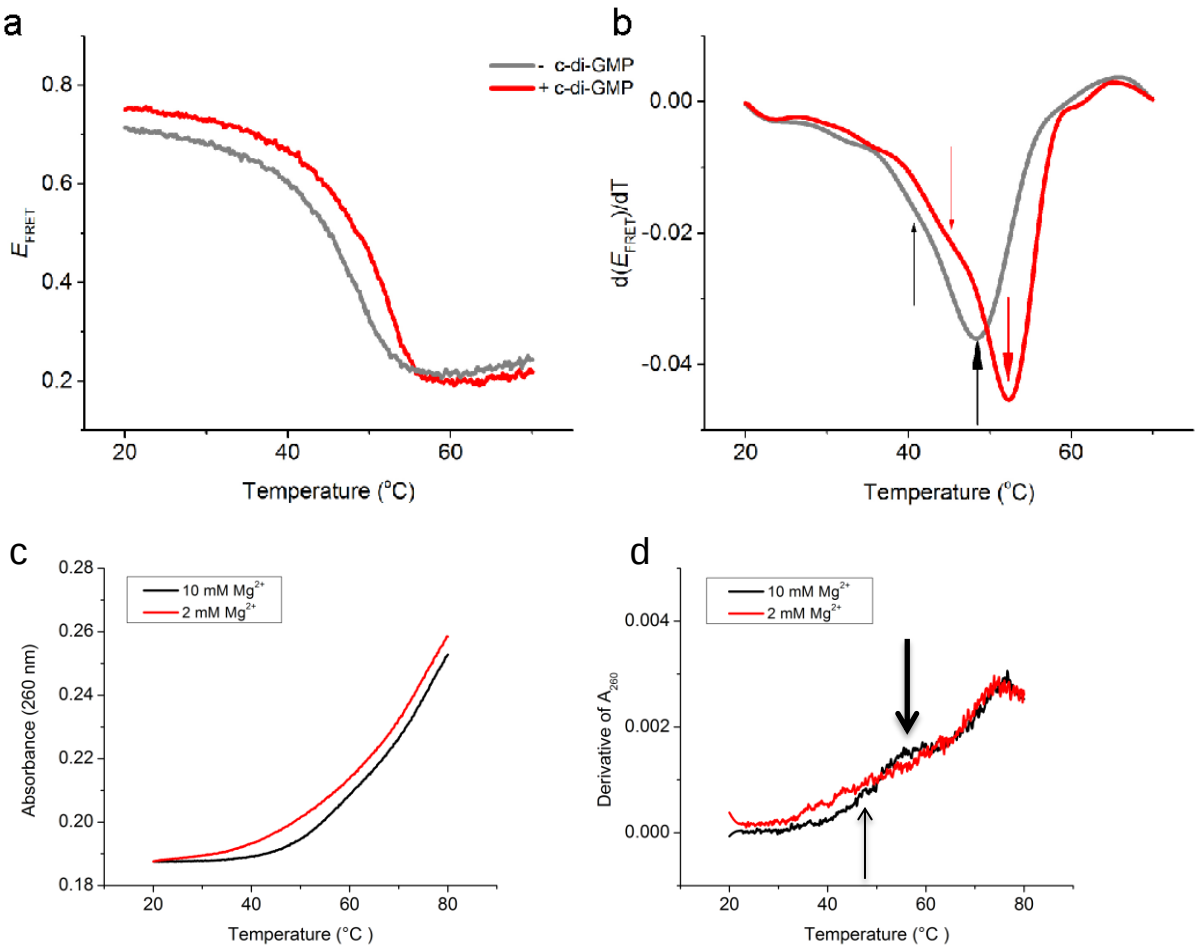


**Supplementary Figure 9.** Temperature-induced tertiary unfolding may involve two steps. (**a**) Temperature-induced tertiary unfolding of the bimolecular, dual-labeled c-di-GMP riboswitch construct in 25 mM $Mg^{2+}$ monitored by FRET in the absence (black) and presence (red) of c-di-GMP. (**b**) Derivative of the $E_{FRET}$ signal plotted in the absence (black) and presence (red) of c-di-GMP. The $T_m^{3°}$ for each curve is indicated with a thick arrow while a minor, putative unfolding step is indicated with a thin arrow. This initial unfolding event is inferred by the departure from a single Gaussian bell-shape in the derivative plot. (**c**) Thermal unfolding can also be monitored by absorbance at 260 nm using a bimolecular construct lacking fluorophores but otherwise identical to that used in the FRET assay. (**d**) Secondary structure unfolding (duplex melting) occurs at ~74 °C in 2 mM $MgCl_2$ (red), ~78 °C in 10 mM $MgCl_2$ (black). The $A_{260}$ derivative reproducibly exhibits two small features within the tertiary unfolding peak, denoted with arrows (~48 ºC and ~56 ºC) in 10 mM $Mg^{2+}$. These features may correspond to a two-step tertiary unfolding process.

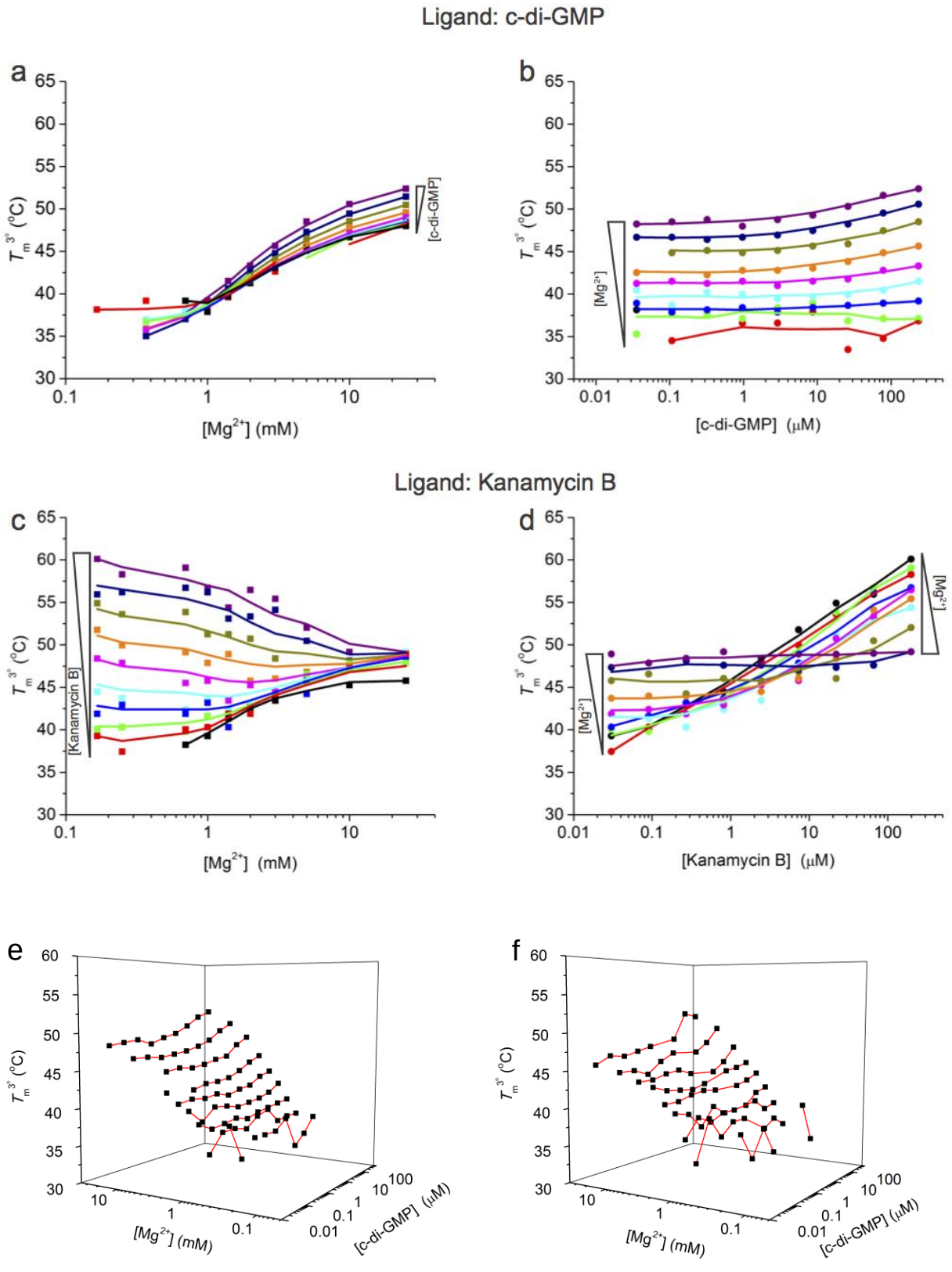
Ligand: c-di-GMP
a
b
$T_m^{3°}$ (°C)
[Mg2+] (mM)
[c-di-GMP]
[Mg2+]
[c-di-GMP] (μM)
Ligand: Kanamycin B
c
d
[Kanamycin B]
[Mg2+] (mM)
[Kanamycin B] (μM)
e
f
[Mg2+] (mM)
[c-di-GMP] (μM)

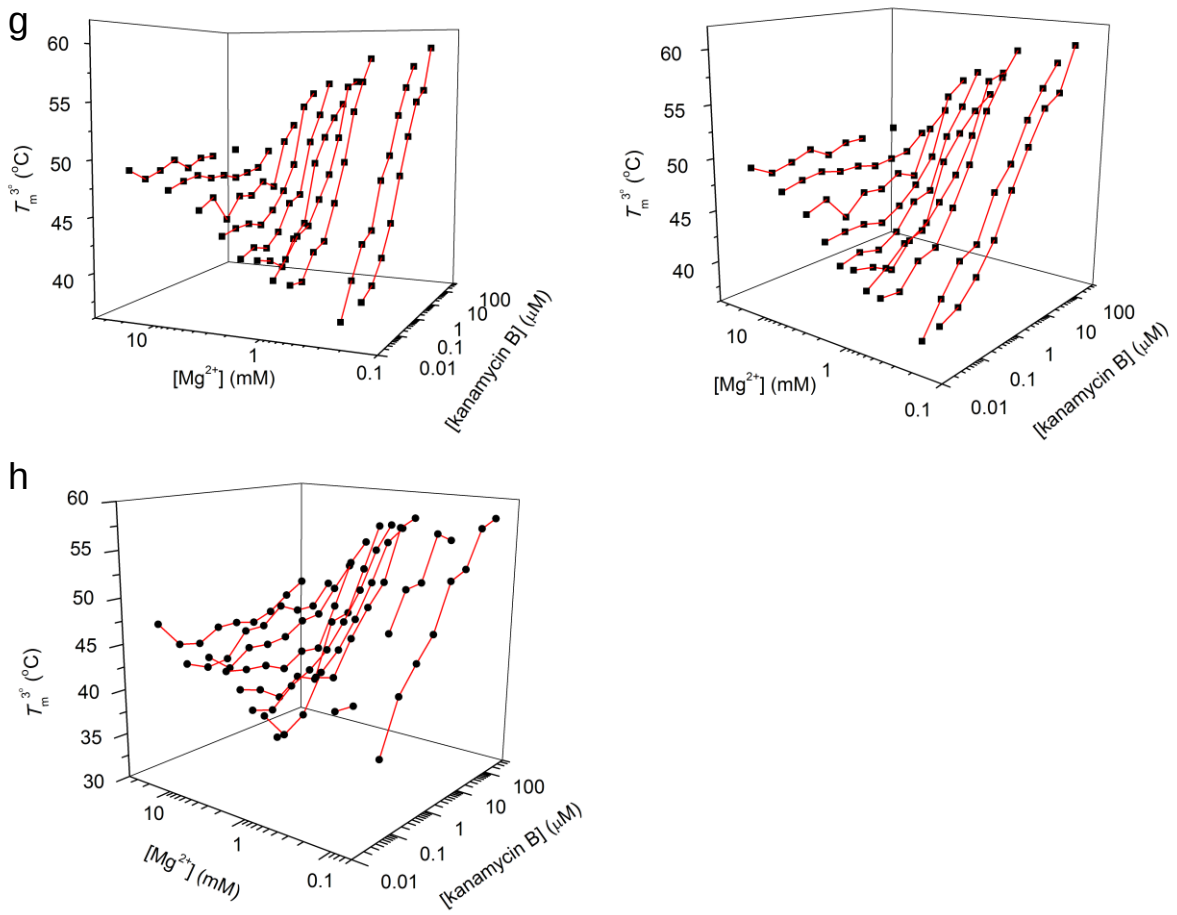


**Supplementary Figure 10.** Two-dimensional and three-dimensional plots of $T_m^{3°}$ as a function of $Mg^{2+}$ and ligand. Lines represent data smoothed using Adjacent-Averaging (Origin 9.1). (**a**) $T_m^{3°}$ as a function of $Mg^{2+}$ titration in the presence of different c-di-GMP concentrations (all in μM; 0, black; 0.035, red; 0.11, green; 0.32, blue; 0.96, cyan; 2.9, magenta; 8, orange; 26, olive; 78, navy; 235, purple). (**b**) $T_m^{3°}$ as a function of c-di-GMP titration in the presence of different $Mg^{2+}$ concentrations (all in mM; 0.37, red; 0.7, green; 1, blue; 1.4 cyan; 2, magenta; 3, orange; 5, olive; 10, navy; 25 purple). In all $Mg^{2+}$ concentrations that supported c-di-GMP binding the $T_m^{3°}$ increased in the presence of c-di-GMP. (**c**) $T_m^{3°}$ as a function of $Mg^{2+}$ titration in the presence of different kanamycin B concentrations (all in μM; 0, black; 0.03, red; 0.09, green; 0.27, blue; 0.81, cyan; 2.4, magenta; 7.3, orange; 22, olive; 66, navy;

198, purple). The $T_m^{3^o}$ in the presence of kanamycin B was highly dependent on $Mg^{2+}$ concentration. At low $Mg^{2+}$ concentrations, addition of high kanamycin B concentrations increased the $T_m^{3^o}$ significantly. At high $Mg^{2+}$ concentrations, the addition of high kanamycin B concentrations did not change the $T_m^{3^o}$, within experimental error, suggesting that an RNA conformation is stabilized that is not competent to bind kanamycin B. (**d**) $T_m^{3^o}$ as a function of kanamycin B titration in the presence of different $Mg^{2+}$ concentrations (all in mM; 0.167m black; 0.25, red; 0.7, green; 1, blue; 1.4 cyan; 2, magenta; 3, orange; 5, olive; 10, navy; 25 purple). In 25 mM $Mg^{2+}$ the $T_m^{3^o}$ was identical in the absence and presence of kanamycin B suggesting that the thermal stability was not even affected by the non-specific positive charge of the aminoglycoside. Stability landscapes in the presence of c-di-GMP (**e**) from the experiment depicted in **Fig. 5a** and (**f**) from an experiment prepared with different samples on a different day are reproducible across the range of experimental conditions. The $Mg^{2+}$ and kanamycin B concentration ranges are slightly different between the two experiments, precluding direct averaging of the data. In both landscapes, the data at lowest $Mg^{2+}$ concentrations exhibit larger variations in $T_m^{3^o}$ as a result of very low $\Delta E_{FRET}$ signal during thermal unfolding. (**g**) Multiple orientations of the stability landscape depicted in **Fig. 5b** reveal the overall shape and demonstrate the overall incongruence with the conformational landscape shown in **Fig. 3a**. Stability landscapes in the presence of kanamycin B from experiments prepared with different samples on different days are reproducible, as shown in (**g**) and (**h**). The $Mg^{2+}$ and kanamycin B concentration ranges are slightly different between the two experiments, precluding direct averaging of the data.

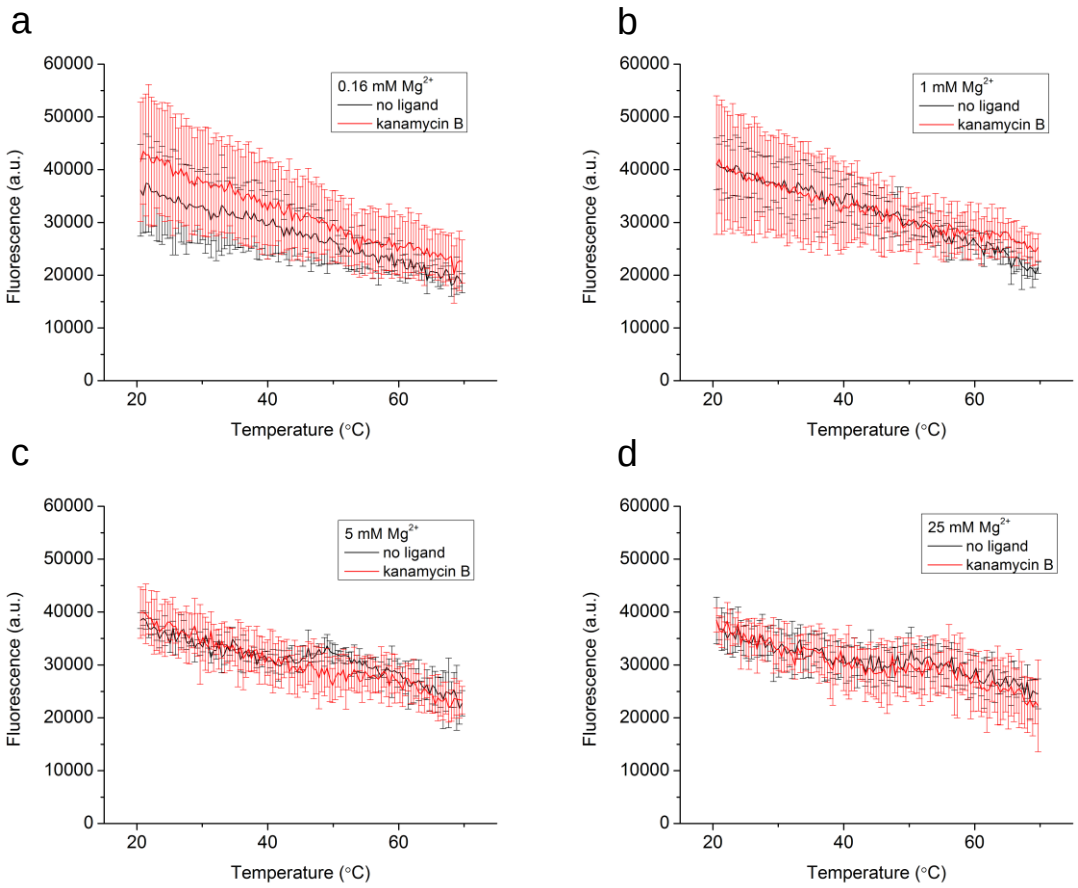


**Supplementary Figure 11**. Temperature-dependent fluorescence of Cy3-labeled RNA. Within experimental error, the fluorescence of a Cy3-labeled bimolecular RNA construct is identical in the absence and presence of 200 μM kanamycin B. This demonstrates that kanamycin B does not alter the fluorescence properties of Cy3 across the temperature range in (**a**) 0.16 mM $Mg^{2+}$, (**b**) 1 mM $Mg^{2+}$, (**c**) 5 mM $Mg^{2+}$, and (**d**) 25 mM $Mg^{2+}$. The bimolecular RNA construct used in this experiment is identical to that used in the FRET experiments except only the Cy3 fluorophore is incorporated. Each experiment was performed in triplicate and is reported as the mean ± standard deviation.

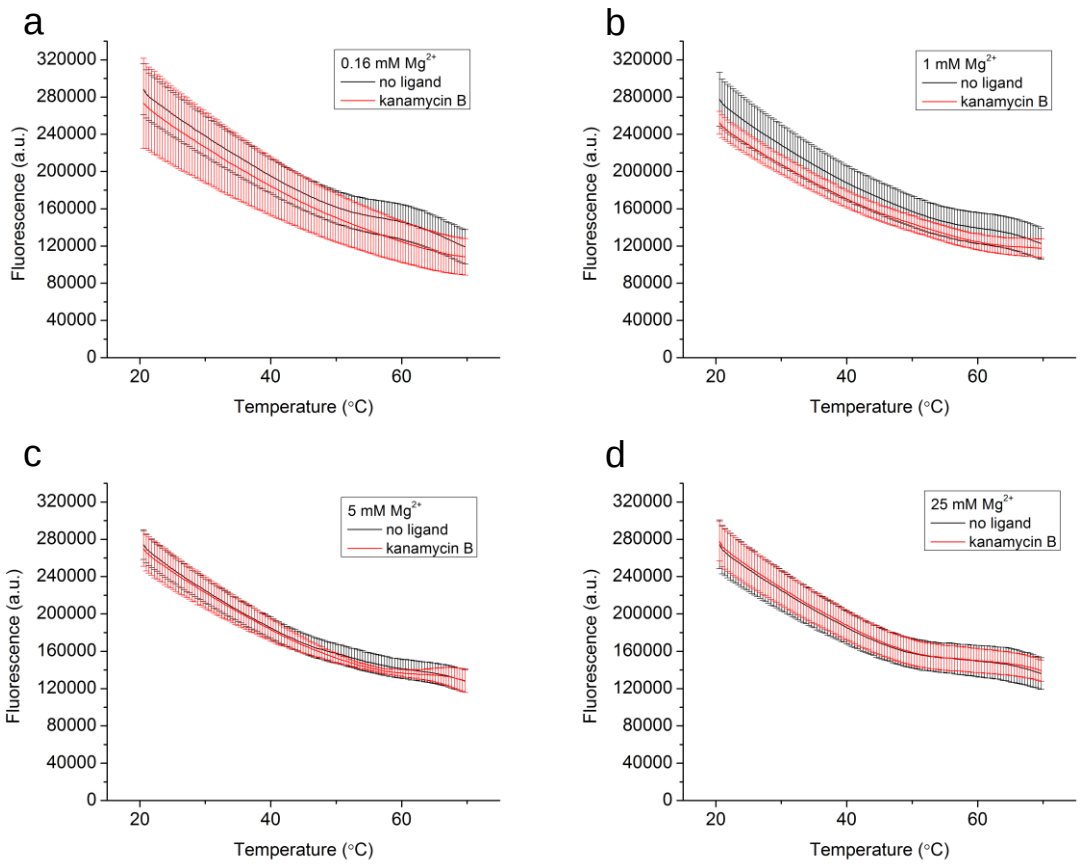


**Supplementary Figure 12**. Temperature-dependent fluorescence of Cy5-labeled RNA. Within experimental error, the fluorescence of Cy5-labeled bimolecular RNA construct is identical in the absence and presence of 200 μM kanamycin B. This demonstrates that kanamycin B does not alter the fluorescence properties of Cy5 across the temperature range in (**a**) 0.16 mM $Mg^{2+}$, (**b**) 1 mM $Mg^{2+}$, (**c**) 5 mM $Mg^{2+}$, and (**d**) 25 mM $Mg^{2+}$. The bimolecular RNA construct used in this experiment is identical to that used in the FRET experiments except that only the Cy5 fluorophore is incorporated. Each experiment was performed in triplicate and is reported as the mean ± standard deviation.

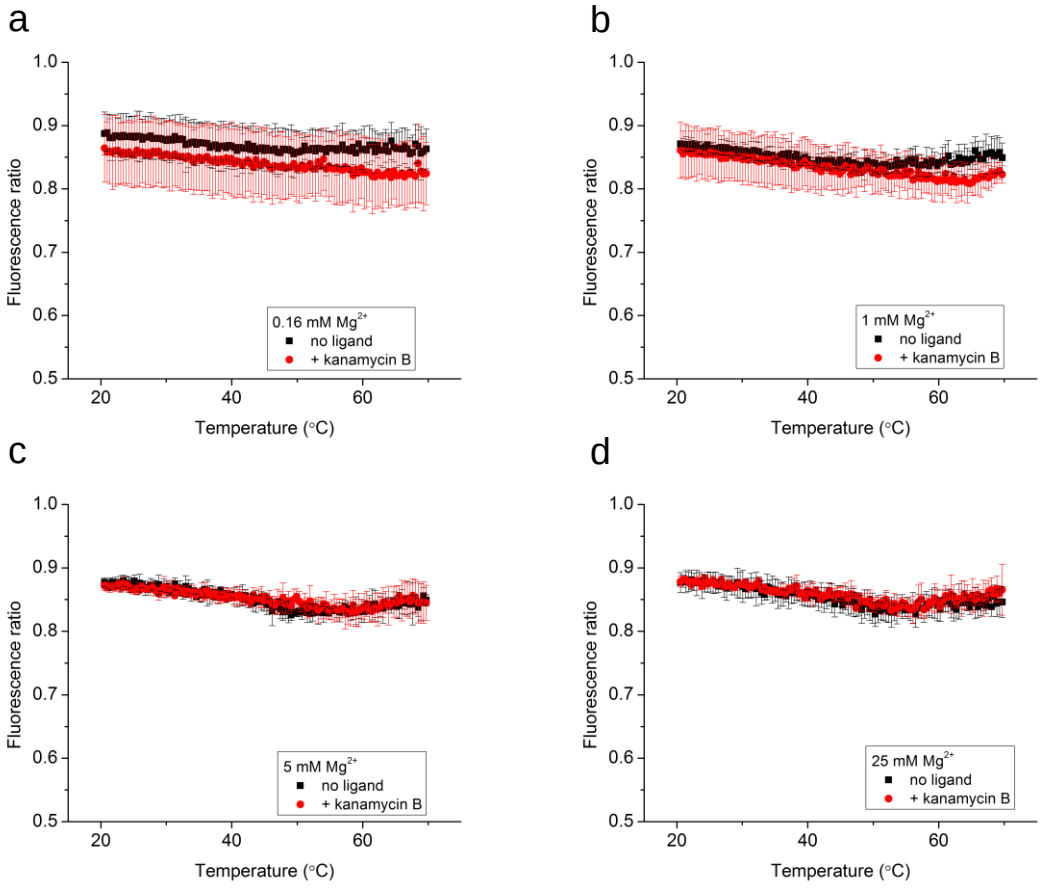


**Supplementary Figure 13**. Temperature-dependent fluorescence ratio. A pseudo-$E_{FRET}$ [Cy5/(Cy5+Cy3)] was calculated from the two singly-labeled RNAs (**Supplementary Figs. 11** and **12**). Within error, the pseudo-$E_{FRET}$ is identical in the absence and presence of 200 μM kanamycin B in (**a**) 0.16 mM $Mg^{2+}$, (**b**) 1 mM $Mg^{2+}$, (**c**) 5 mM $Mg^{2+}$, and (**d**) 25 mM $Mg^{2+}$. Generally, the pseudo-$E_{FRET}$ decreases slightly and monotonically over the temperature range. At high [$Mg^{2+}$], the pseudo $E_{FRET}$ increases slightly above ~60 °C. The slight changes in pseudo-$E_{FRET}$ from these control experiments do not complicate interpretation of the $E_{FRET}$ changes in the doubly-labeled RNA (**Supplementary Figs. 7** and **8**), wherein the observed $E_{FRET}$ decreases cooperatively, not monotonically, upon unfolding, even at temperatures near 60 °C (**Supplementary Fig. 8c**). Each calculated pseudo- $E_{FRET}$ was performed in triplicate and is reported as the mean ± standard deviation.

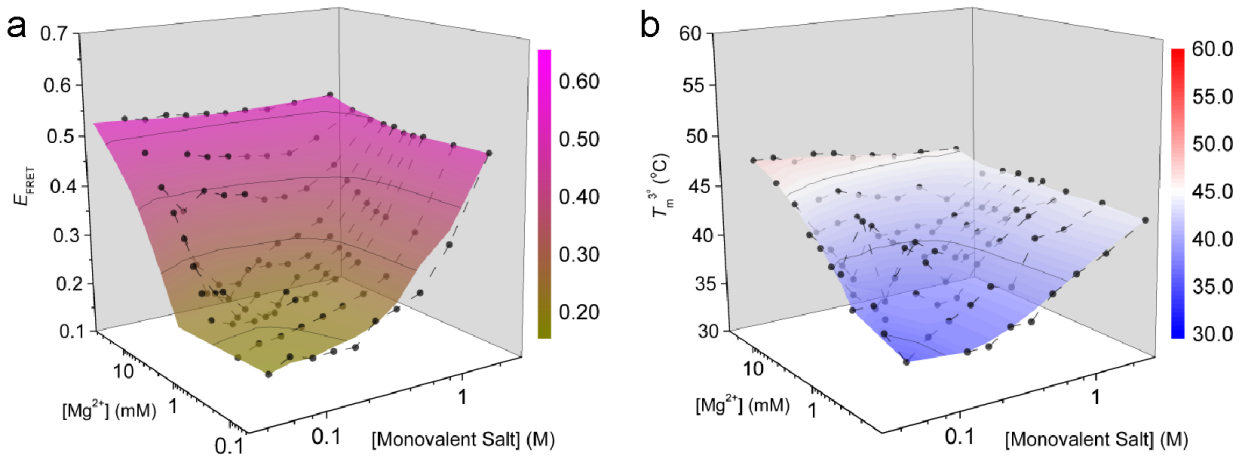


**Supplementary Figure 14.** $E_{FRET}$ and $T_m^{3°}$ landscapes of the c-di-GMP riboswitch as a function of increasing ionic strength. (**a**) The $E_{FRET}$ landscape demonstrates that both $Mg^{2+}$ and monovalent salts (equimolar $Na^+$ and $K^+$) promote the folded conformation. (**b**) The shape of the $T_m^{3°}$ landscape is similar to the $E_{FRET}$ landscape and indicates that charge neutralization by up to 2 M monovalent salts does not result in an increased $T_m^{3°}$ beyond that obtained with $Mg^{2+}$ alone. Comparison of these landscapes with those obtained in the presence of kanamycin B (**Figs. 3** and **5**) indicate that charge neutralization is not solely responsible for the alternative conformation stabilized by kanamycin B.

**Supplementary Tables**

**Supplementary Table 1.** Single point $E_{FRET}$ in the absence and presence of c-di-GMP

| Ligand: | none | c-di-GMP |
|---|---|---|
| 1 mM $Mg^{2+}$ (± 0.02) | 0.30 | 0.41 |
| 10 mM $Mg^{2+}$ (± 0.01) | 0.53 | 0.62 |

**Supplementary Table 2.** Single point $E_{FRET}$ in the absence and presence of kanamycin B

| Ligand: | none | Kanamycin B |
|---|---|---|
| 1.1 mM $Mg^{2+}$ (± 0.02) | 0.31 | 0.33 |
| 10 mM $Mg^{2+}$ (± 0.01) | 0.53 | 0.48 |

**Supplementary Table 3.** Thermodynamic parameters obtained by ITC titration of c-di-GMP in the absence or presence of kanamycin B.

| | | **2 mM $Mg^{2+}$** | | **10 mM $Mg^{2+}$** | |
|---|---|---|---|---|---|
| | kanamycin B: | none | 200 μM | none | 200 μM |
| $K_D$ | (μM) | 0.978 | 1.350 | 0.270 | 0.378 |
| $\Delta H$ | (kcal/mol) | -12.51 | -14.03 | -9.79 | -10.42 |
| $-T\Delta S$ | (kcal/mol) | 4.45 | 6.16 | 0.98 | 1.81 |
| $\Delta G$ | (kcal/mol) | -8.06 | -7.87 | -8.81 | -8.62 |

**Supplementary Notes**

**Supplementary Note 1.** Analysis of kanamycin B titrations. The biphasic kanamycin B-induced $E_{FRET}$ responses precluded analysis using a simple two-state model. Given the unusual shape of the conformational landscape, we did not extrapolate end-points assuming monotonic $E_{FRET}$ increases or decreases (at higher kanamycin B concentrations). Indeed, at higher kanamycin B concentrations additional non-monotonic $E_{FRET}$ responses may exist. We therefore did not fit the ten kanamycin B titrations to any binding model.

**Supplementary Note 2.** Advantages of FRET thermal melts over traditional DSF experiments. Differential scanning fluorimetry, or DSF, experiments characterize ligand-conferred protein stability[4,5]. Given its easy adaptation to high-throughput instrumentation, the assay has been adopted for chemical screening against protein targets; active compounds induce a shift in thermal unfolding ($T_m$). The fluorescence signal is generated from an exogenous ligand whose emission is significantly increased upon binding hydrophobic patches exposed during protein unfolding. Potential drawbacks to traditional DSF experiments arise from the non-specific protein-dye interaction. First, an optimization step is required to identify the combination of protein and dye concentrations yielding robust signal changes. Second, some protein-dye pairs interact only weakly, resulting in small or indiscernible signal changes in the melting curve. In such cases, an alternative dye must be employed. Third, due to the random association of the dye with the protein, the thermally-induced transition cannot be structurally interpreted.

To avoid these drawbacks of traditional DSF, we developed a differential scanning FRET assay with two rationally positioned fluorescent dyes that are covalently attached to the RNA. Based on prior knowledge of the 3D structure and folding of the RNA, the location of the dyes ensures a FRET signal concomitant with folding. Furthermore, the fluorescence changes during thermal melting are not dependent on an interaction between the dye and the RNA. The dyes fluoresce under all temperatures probed and their signal change reports on the conformational change in the RNA.

**Supplementary Note 3.** $T_m^{3^\circ}$, a tertiary thermal unfolding parameter. We reported the $T_m^{3^\circ}$, or tertiary unfolding temperature, from each thermal unfolding curve. We used the $T_m^{3^\circ}$ notation rather than the more conventional $T_m$ notation for two reasons. First, our assay monitors tertiary RNA unfolding and needs to be distinguished from the more common qPCR application of measuring DNA duplex melting for genotyping single-nucleotide polymorphisms. Second, our FRET construct and experimental temperature range (<70 °C) only evaluated the tertiary melting transition; the duplex melting transition occurs around ~76 ºC (**Supplementary Fig. 9d**).

**Supplementary Note 4**. Error in the $T_m^{3^\circ}$ measurement. The $T_m^{3^\circ}$ landscape is generated by calculating the derivative of the $E_{FRET}$ signals over 194 temperatures for each of the 100 multiplexed solution conditions. The high-frequency noise in the $E_{FRET}$ measurements (**Fig. 4** and **Supplementary Fig. 6**) is inconsequential when the overall $E_{FRET}$ signal change is large. However, when the overall $E_{FRET}$ signal change is very small (*e.g.* the lowest $Mg^{2+}$ concentrations in presence of c-di-GMP), this high-frequency noise becomes significant and leads to increased error in the $T_m^{3^\circ}$ derivative calculation. The lower signal-to-noise ratio for $T_m^{3^\circ}$ measurements at low $Mg^{2+}$ concentrations results in minor differences in the shape of the c-di-GMP thermal stability landscape relative to the shape of the c-di-GMP

conformation landscape. These differences are not physically meaningful, but demonstrate the limitations of $T_m^{3^\circ}$ measurements when the $\Delta E_{FRET}$ signal is small.

**Supplementary Note 5**. Coupling and uncoupling of RNA conformation and thermal stability. The thermodynamic hypothesis of macromolecular (protein and RNA) folding[6] asserts that the native state represents a global minimum of free energy. Hence, folded conformations and their free energy are directly linked. Therefore, the conformation and stability of productive folding intermediate states are necessarily intermediate between those of the unfolded and folded states. In contrast, non-productive trapped intermediates do not simply transition along the pathway between unfolded and folded states. They may be topologically constrained[7] or may be stabilized by non-native contacts with a protein or small molecule ligand[8]. In either case, the thermal stability of those intermediates is not inherently coupled to those of the natively folded and unfolded states. This uncoupling may result in disparate measurements of conformation, stability, or specific activity.

In our study, the incongruent $E_{FRET}$ and $T_m^{3^\circ}$ landscapes observed for the riboswitch-kanamycin B interaction demonstrate that the folding and stability have been uncoupled. We interpret this to be caused by a non-productive intermediate stabilized by kanamycin B. In contrast, coincident conformational and thermal stability landscapes were observed in the presence of cyclic di-GMP. This coupling between folding and stability is consistent with the absence of off-pathway intermediates.

**Supplementary Note 6.** Non-cognate ligand binding is highly dependent on $Mg^{2+}$ concentration. The conformational and stability landscapes reveal that kanamycin B binding is precluded at high $Mg^{2+}$

conditions (25 mM). Stated otherwise, the $Mg^{2+}$-stabilized state is not disrupted by up to 200 μM kanamycin B. High $Mg^{2+}$ conditions screen the affect even of non-specific charge interactions (kanamycin B has five positively charged amino groups at neutral pH) such that the $T_m^{3^\circ}$ is nearly unchanged by the addition of kanamycin B in 25 mM $Mg^{2+}$ (**Supplementary Fig. 10**). In contrast, the riboswitch-kanamycin B interaction observed under low $Mg^{2+}$ conditions, where c-di-GMP does not bind, results at least in part from the positive charge of the aminoglycoside. The strong $Mg^{2+}$ dependence of the RNA-kanamycin B interaction highlights the importance of choosing appropriate solution conditions when screening for novel ligand-RNA interactions. Non-cognate ligands are likely to bind metastable conformations, whose structures are not accessible under highly stabilizing conditions.

**Supplementary Note 7.** Obtaining conformational and stability landscapes from a single instrument read. To generate conformational landscapes we measured fluorescence intensities with minimal noise reliably down to 15 nM RNA (20 μL) using a microplate fluorometer. Fluorescence measurements using a qPCR machine under similar conditions yielded significantly noisier $E_{FRET}$ measurements. However, using 40 nM RNA in 25 μL we recorded high quality $E_{FRET}$ measurements on the qPCR machine for $Mg^{2+}$ titrations in the absence and presence of c-di-GMP. The quality of these data produced fits to the two $Mg^{2+}$ titrations in agreement with data obtained from the microplate fluorometer. Preparation of samples in this way will allow for robust measurement of all four parameters ($E_{FRET}$, $K_{Mg}$, $K_D$, and $T_m^{3^\circ}$) and generation of conformational and stability landscapes in a single experiment using a single read on a qPCR machine.

**Supplementary References**


1 Wood, S., Ferré-D'Amaré, A. R. & Rueda, D. Allosteric tertiary interactions preorganize the c-di-GMP riboswitch and accelerate ligand binding. *ACS Chem Biol* **7**, 920-927 (2012).

2 Smith, K. D., Lipchock, S. V., Livingston, A. L., Shanahan, C. A. & Strobel, S. A. Structural and biochemical determinants of ligand binding by the c-di-GMP riboswitch. *Biochemistry* **49**, 7351-7359 (2010).

3 Kulshina, N., Baird, N. J. & Ferré-D'Amaré, A. R. Recognition of the bacterial second messenger cyclic diguanylate by its cognate riboswitch. *Nat Struct Mol Biol* **16**, 1212-1217 (2009).

4 Niesen, F. H., Berglund, H. & Vedadi, M. The use of differential scanning fluorimetry to detect ligand interactions that promote protein stability. *Nat Protoc* **2**, 2212-2221 (2007).

5 Pantoliano, M. W. *et al.* High-density miniaturized thermal shift assays as a general strategy for drug discovery. *J Biomol Screen* **6**, 429-440 (2001).

6 Epstein, C. J., Goldberger, R. F. & Anfinsen, C. B. The Genetic Control of Tertiary Protein Structures: Studies with Model Systems. *Cold Spring Harbor Symp Quant Biol* **28**, 439-449 (1963).

7 Chen, C. *et al.* Understanding the role of three-dimensional topology in determining the folding intermediates of group I introns. *Biophys J* **104**, 1326-1337 (2013).

8 Grohman, J. K. *et al.* An immature retroviral RNA genome resembles a kinetically trapped intermediate state. *J Virol* **88**, 6061-6068 (2014).